Hindawi
Shock and Vibration
Volume 2019, Article ID 6813693, 12 pages
https://doi.org/10.1155/2019/6813693

Research Article

Peak Response Prediction for RC Beams under Impact Loading

Wuchao Zhao, Jiang Qian, and Pengzhao Jia

State Key Laboratory of Disaster Reduction in Civil Engineering, Tongji University, Shanghai 200092, China

Correspondence should be addressed to Jiang Qian; jqian@tongji.edu.cn

Received 7 October 2018; Revised 16 December 2018; Accepted 31 December 2018; Published 22 January 2019

Academic Editor: Mohammad Rafiee

In this paper, a novel and simple method for predicting the peak response of RC beams subjected to impact loading is proposed. The theoretical basis for calculating the peak impact force originates from the contact law, the principle of conservation of energy, the impulse-momentum theorem, and the wave theory. Additionally, the conventional beam theory, in conjunction with the well-known layered-section approach, is utilized to obtain the force-deflection relationship of the RC beam. Subsequently, by taking into account the strain rate effect, the maximum midspan deflection of RC beams under impact loading is determined based on the conservation of energy approach. A comparison with 143 impact tests has shown that the proposed method is able to estimate the maximum midspan deflection of RC beams under impact loading with high accuracy. The prediction of the peak impact force is shown to be slightly overestimated, which however can be used in the anti-impact design to preclude the shear failure near the impact point.

1. Introduction

RC components widely used in the construction of buildings and civil infrastructures may be threatened by various types of impact loadings during their service life, such as vehicle collisions, rockfall impacts, and terrorist attacks. Concrete structures have been commonly used as protective ones in order to resist the extreme loads. In the past two decades, the dynamic response of RC elements under impact loading has been the subject of many studies [1–5], devoted to illustrating the impact mechanism. Due to the intense energy released in an extremely short time, the dynamic response and failure mode are different for RC beams under impact and quasistatic loads. Moreover, due to the nature of the impact process, the time-history response of the system is not very important compared with the peak response. Thus, it is crucial to establish simplified methods for reliably predicting the peak response of RC components under impact loading.

Previous studies have indicated that RC beams subjected to impact loading usually undergo a local response phase and an overall response phase [1]. In the local response phase, a shear-plug is expected to form near the impact point [6, 7], which is mainly triggered by the high peak impact force during the first impact impulse. Many impact tests have shown that shear cracks will develop at the impact point before any noticeable bending occurs [8]. Therefore, it is recognized that the peak impact force is an important index to evaluate the impact capacity of RC beams. Moreover, the localized damage of the beam, induced by the impact force in the local response phase, promotes the formulation of the plastic hinge at the midspan in the overall response phase. After that, the RC beam gradually reaches its maximum deflection. Thus, the maximum midspan deflection can also be regarded as an important performance index for evaluating the damage degree of RC beams [9, 10]. A number of drop-weight impact tests [2, 6, 7, 10] have been conducted in order to investigate the impact behaviour of RC beams. However, the tested specimens conducted by each scholar are rather limited. In addition, the test technique is still limited owing to the lack of general facility and impact test procedure; different measurement techniques, such as load cells, accelerometers, strain gauges, and high-speed photography, are extensively applied in the impact tests. Hence, it is difficult to obtain a general conclusion from the few available impact tests.

With recent advances in computer technology and finite element (FE) theory, many researchers [11–13] have managed

to model the impact phenomenon and predict the response of RC elements using FE software packages, such as LS-DYNA and ABAQUS. However, the contact algorithms have a significant influence on the prediction of the impact force; therefore, the contact algorithm and the scale factor must be selected with extreme caution [13, 14]. In addition, the dynamic behaviour of concrete under impact loading is very complex, and thus, it is not an easy task to accurately reproduce the actual response. Hence, the need for a more efficient but straightforward method to predict the impact response of RC components is urgent.

To reduce the efforts required for the FE simulation, mass-spring models have been applied to predict the dynamic response of RC beams subjected to localized impact [1, 15, 16]. Even though the simplified models are convenient to apply, the parameters in the models should be determined in advance by the trial-and-error method. In this case, several contact laws have been developed by previous studies [17, 18] to calculate the contact force. However, it is difficult to determine the indentation and contact stiffness with high accuracy because the impact process involves plastic deformation, material degradation, and strain rate effect. In addition, there are some limitations in predicting the transient impact response of RC beams, especially the stress wave propagation. Based on their studies, Pham and Hao [19] and Yi et al. [20] suggested that the impact-induced wave propagation should be taken into account in the local response phase.

In order to quickly predict the peak impact force of RC beams under drop-weight impact, Pham and Hao [3] proposed an empirical model based on the artificial neural network. In terms of the maximum midspan displacement, Kishi and Mikami [10] and Tachibana et al. [2] conducted a series of impact tests on RC beams with different span lengths, cross sections, and longitudinal reinforcements, proposing empirical formulas for the anti-impact design of RC beams following the performance-based design concept. Although yielding relatively accurate predictions for the maximum impact force and deflection, these empirical formulas lack theoretical foundation and strongly rely on the input data.

In view of these issues, a simplified method with the theoretical foundation is established in this paper for predicting both the peak impact force and the maximum midspan deflection of simply supported RC beams under impact loading. Appropriate assumptions and theoretical derivation are performed to establish the simplified method for predicting the maximum impact response of RC beams. Moreover, data from a total of 143 RC beams under impact loading acting at midspan are compiled and utilized to validate the proposed method.

2. Simplified Analysis Method

2.1. Idealized Collision Process. In order to facilitate the derivation process of the simplified method, the time history of impact force is simplified in this study based on previous experimental observations, as presented in Figure 1. It is assumed that the impact force versus time curve can be

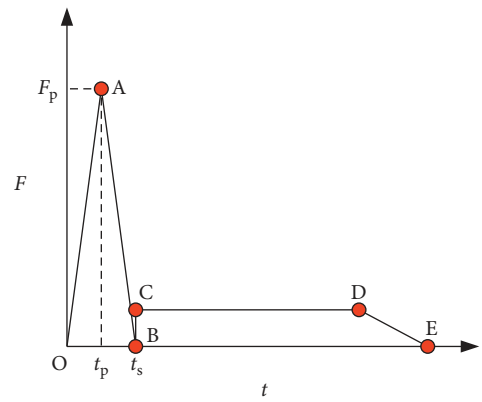

Figure 1: Idealized time history of the impact force.

generally divided into three stages: firstly, the impact force reaches the maximum value (Point A) in a very short time (OA segment) and then descends to a small value which is approximately equal to zero (AB segment). After Point C, the RC beam enters the global response stage, and the value of the impact force nearly remains constant for a relatively long period (CD segment). Finally, the impact force goes into the descending stage and gradually decreases to zero (DE segment). In the global response stage, the elastic-plastic deformation of the RC beam gradually increases until the maximum deflection is reached, and most of the impact energy is absorbed by the RC beams.

Furthermore, the impact force between Point O and Point B is simplified as a triangular pulse. The collision process is schematically presented in Figure 2. For the sake of simplicity, the rise and fall time of the first triangular impulse are assumed to be the same, such as

$$t_s = 2t_p, \tag{1}$$

where t_s is the final time of the first impact impulse and t_p is the time at the peak impact force.

Neglecting the overall deformation of the RC beam, the local indentation reaches its maximum value α_p when the impact force reaches Point A (refers to Figure 2(b)). At this time, the velocities of the impactor and the RC beam are V_1 and V_2, respectively. The following relationship can be derived on the basis of the momentum conservation law:

$$MV_0 = MV_1 + mV_2. \tag{2}$$

Since only a small part of the beam responses to the impact loading at the very beginning of impact, the concept of effective response length [21] is introduced herein. Then, the beam effective mass m is calculated using the approximate design method proposed by Biggs [22]:

$$m = K_m \cdot (\rho_l \cdot l_{eff}) = \frac{\int \rho_l \phi^2(x)dx}{\int \rho_l dx} (\rho_l \cdot l_{eff}), \tag{3}$$

where ρ_l is the mass of the RC beam per length, $\phi(x)$ is the assumed shape function on which the establishment of a generalized single-degree-of-freedom (SDOF) system is based, and l_{eff} is the effective response length of the beam.

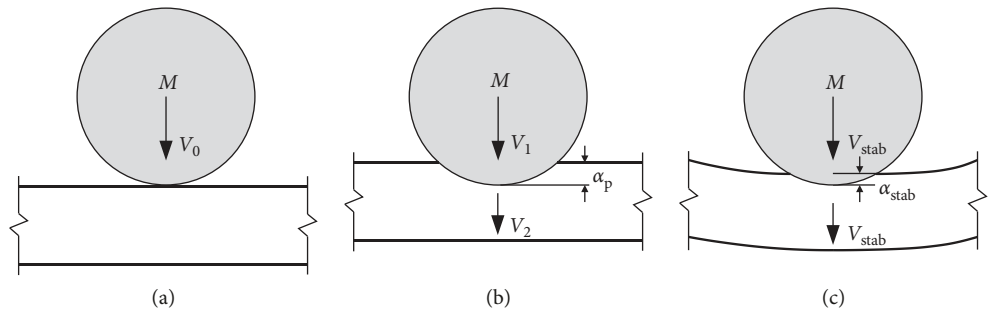

Figure 2: Collision process during the first impact impulse. (a) $t = 0$. (b) $t = t_p$. (c) $t = t_s$.

According to Pham and Hao [23] and Isaac et al. [24], the shape function adopted in this paper is expressed as follows:

$$\phi(x) = \begin{cases} \dfrac{2x}{l_{\text{eff}}}, & 0 \le x \le \dfrac{l_{\text{eff}}}{2}, \\ \dfrac{2(l_{\text{eff}} - x)}{l_{\text{eff}}}, & \dfrac{l_{\text{eff}}}{2} < x \le l_{\text{eff}}. \end{cases} \tag{4}$$

When the impact force reaches Point B, the impactor and the RC beam have the same velocity V_{stab}, which can be obtained from the following equation:

$$V_{\text{stab}} = \frac{MV_0}{(M+m)}. \tag{5}$$

Based on equation (1) and the linear impulse-momentum law, the velocities of the impactor and the beam at the peak impact force can be calculated as follows:

$$V_1 = \frac{1}{2}(V_{\text{stab}} + V_0), \tag{6}$$

$$V_2 = \frac{1}{2}V_{\text{stab}}. \tag{7}$$

2.2. Contact Model. It is known that the Hertz contact model cannot be applied to describe the relationship between the impact force and the local indentation when the contact surface is flat. Moreover, the difficulties of the elastic contact stress theory are that the displacement at any point on the contact surface depends on the distribution of the pressure throughout the whole contact [25].

To overcome these difficulties, Lu and Yu [25] suggested that the impacted solids can be simulated using a simple Winkler elastic foundation rather than an elastic half-space, as shown in Figure 3. The indentation α can be written in terms of the radius of the impactor, R, and the contact radius, a, as

$$\alpha = R - \left(R^2 - a^2\right)^{1/2}. \tag{8}$$

In general, the indentation is much smaller than the radius of the impactor. Thus, equation (8) can be rewritten as

$$\alpha = \frac{a^2}{2R}. \tag{9}$$

The deformations under the impactor can be written as

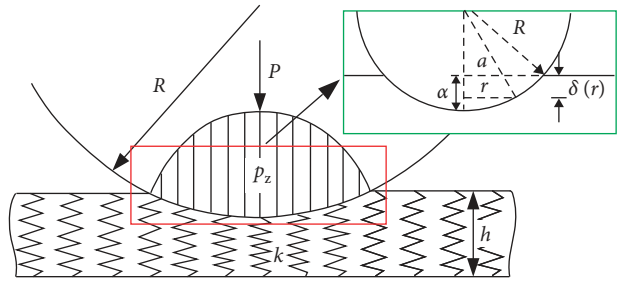

Figure 3: Winkler elastic foundation model.

$$\delta(r) = \alpha - \left(R - \left(R^2 - r^2\right)^{1/2}\right). \tag{10}$$

Similarly, the second term of the right-hand side of the above equation can be simplified as $(r^2/2R)$. Therefore, equation (10) takes the form

$$\delta(r) = \alpha - \frac{r^2}{2R}. \tag{11}$$

Assuming that the material behaves elastically, the contact force is expressed as

$$F = 2\pi k \int \delta(r) r\, dr, \tag{12}$$

where $k = E/h$ is the stiffness of the foundation spring.

Substituting equations (9) and (11) into equation (12), the relationship between the contact force and the indentation can be described by

$$F(\alpha) = \frac{\pi \text{ER}}{h}\alpha^2. \tag{13}$$

Similarly, the contact force between a flat impactor nose and a RC beam can be calculated by

$$F(\alpha) = \frac{EA}{h}\alpha, \tag{14}$$

where A is the area of the contact surface.

It is well known that the impact problems not only involve the elastic and plastic deformation but also involve viscosity, hardening, and other complex physical phenomena. However, in order to avoid complicated calculations and hence to provide a simplified method, the contact law adopted in this study is based on the elastic theory.

2.3. Peak Impact Force. The peak impact force usually occurs in one or two milliseconds at the very beginning of impact, and the beam deformations mainly concentrate at the impact point due to the inertial effect. Besides, the deformations under the contact surface are very complex, and even some small cracks appear at this region. For simplicity, it is assumed that the heat, sound, light, and other kinds of energy loss are restored in the contact surface, similar to the contact spring in the previous mass-spring models. Thus, the energy-balance equation can be expressed as

$$\frac{1}{2}MV_0^2 - \frac{1}{2}MV_1^2 - \frac{1}{2}mV_2^2 = E_{sp}, \tag{15}$$

where E_{sp} is the energy stored in the local contact zone; it is given by the following equation:

$$E_{sp} = \int F(\alpha)d\alpha. \tag{16}$$

Substituting equations (5)–(7), (13), and (16) into equation (15), for the impactor with a spherical nose, the peak impact force can be estimated by the following equation:

$$F_p = \left[\frac{9MV_0^2}{8(M/(m+1))}\left(\frac{\pi ER}{h}\right)^{1/2}\right]^{2/3}. \tag{17}$$

Similarly, substituting equations (5)–(7), (14), and (16) into equation (15), the peak impact force generated by the impactor with a flat nose can be obtained by the following equation:

$$F_p = \left(\frac{3MV_0^2}{4(M/(m+1))}\cdot\frac{EA}{h}\right)^{1/2}. \tag{18}$$

Meanwhile, the duration of the first triangular impulse can be calculated by the following equation:

$$t_s = \frac{2M(V_0 - V_{stab})}{F_p}. \tag{19}$$

During the impact process, the stress waves firstly propagate between the top and bottom surfaces in the impact region; meanwhile, the shear waves propagate along the beam length, as shown in Figure 4. Many previous studies [21, 23, 24] have indicated that the shear wave has the most significant effect on the local response of the beam under impact loading, compared to other types of stress waves. When the shear waves have not reached the supports, the effective participation mass of the beam will be less than that calculated by Biggs method [22]. Moreover, according to some impact test results [1], it can be found that the time to reach peak impact force is shortened with the increasing impact velocity, which also results in the reduction in the effective mass of the beam. Therefore, the concept of effective response length is introduced to modify the beam effective mass.

The velocity at which the shear wave travels within the concrete medium [26] is given by the following equation:

$$v_s = \sqrt{\frac{E_c}{(2\rho(1+\mu))}}, \tag{20}$$

where ρ is the density of concrete and μ is the Poisson ratio.

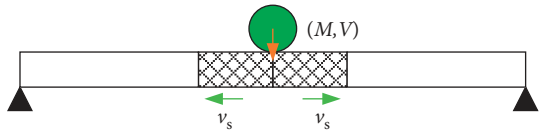

Figure 4: Propagation of stress waves in RC beams.

The propagation distance of shear waves l_s at the peak impact force is obtained by the following equation:

$$l_s = 2v_s t_p. \tag{21}$$

The effective participation mass of the beam can be determined by the relation between the distance covered by shear waves l_s and the beam length l. According to Cotsovos [21] and Pham and Hao [23], the calculation of the effective response length l_{eff} is divided into the following three cases shown in Figure 5: (a) when the shear waves have not reached the supports, the effective response length l_{eff} is taken as l_s, and therefore, the effective mass of the beam is $1/3\rho_l l_s$; (b) when l_s is greater than the net span length l_n but less than the beam length l, the effective response length l_{eff} is taken as the net span length, and the beam effective mass is $1/3\rho_l l_n$; and (c) when l_s is greater than the beam length l, the effective response length l_{eff} is taken as the beam length l, and the beam effective mass can be calculated by equations (3) and (4).

The steps for calculating the peak impact force are summarized schematically as the flowchart in Figure 6.

2.4. Energy-Absorption Capacity of RC Beams. In the overall response stage, the midspan displacement of the beam gradually increases and the deformation mode is similar to that under static force. Moreover, the effect of the wave propagation on the beam response is insignificant and can be ignored. In this case, based on energy equilibrium, the maximum deflection of the beam is calculated including the strain rate effect. Before predicting the maximum midspan deflection, the moment-curvature diagram and the force-deflection diagram should firstly be obtained. Therefore, the energy-absorption capacity of RC beams under dynamic forces is estimated herein with the aid of MATLAB routines developed by the authors.

2.4.1. Constitutive Models. The constitutive model proposed by Hognestad [27] is utilized to simulate the uniaxial stress-strain relation of concrete, as presented in Figure 7(a). The stress-strain relation in compression is described by two regions:

$$\sigma_c = f_c\left[2\left(\frac{\varepsilon_c}{\varepsilon_0}\right) - \left(\frac{\varepsilon_c}{\varepsilon_0}\right)^2\right], \quad \varepsilon \le \varepsilon_0,$$
$$\sigma_c = f_c\left(1 - 0.15\left(\frac{\varepsilon - \varepsilon_0}{\varepsilon_u - \varepsilon_0}\right)\right), \quad \varepsilon_0 < \varepsilon \le \varepsilon_u, \tag{22}$$

where $\varepsilon_0 = 2(f_c/E_c)$ is the concrete strain at maximum stress; E_c is the initial tangent modulus (MPa), which is

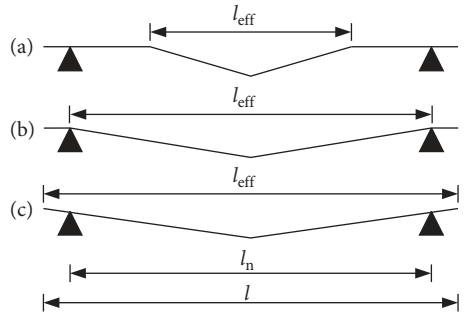

Figure 5: Determination of the effective response length.

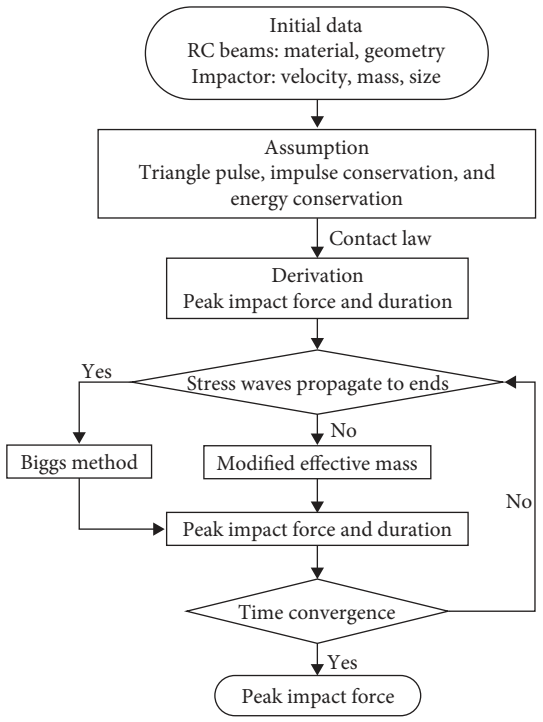

Figure 6: Flowchart for calculating the peak impact force.

assumed the same for both the compressive and tension regimes; ε_u is the ultimate compressive strain and taken as 0.0035; f_c is the compressive strength of concrete (MPa). It is also assumed that the concrete layer with compressive strain beyond ε_u has completely lost its compressive strength.

The elastic modulus of concrete is estimated by the following formula [28]:

$$E_c = 5000\sqrt{f_c}\ (\text{MPa}). \tag{23}$$

The above constitutive model assumes that the tension region of concrete is linearly elastic; thus, the tensile strength f_t can be obtained by $f_t = 0.3\,(f_c)^{2/3}$ [29], while the ultimate tensile strain ε_{tu} is taken as 0.0004.

A linear elastic and strain hardening material is adopted to model reinforcing steels, as shown in Figure 7(b). E_{s1}, f_y, E_{s2}, and ε_u represent Young's modulus, the yield strength, the strain hardening modulus, and the ultimate strain of steel, respectively. For convenience, the constitutive model is assumed to be symmetrical in both compression and tension regimes.

2.4.2. Strain Rate Effect. Numerous experimental and numerical studies [8, 30, 31] have indicated that both strength and deformation characteristics of concrete and reinforcements under dynamic loadings are greatly different from those under static loadings. Therefore, the constitutive properties of these materials over a wide range of strain rates should be taken into consideration. The dynamic increase factor (DIF) (i.e., ratio of the dynamic strength to the static strength) is often utilized to characterize the strain rate effect of structural materials in numerical analyses, as recommended by CEB code 2010 [29].

The relationship between the strain rate $\dot{\varepsilon}$ and the midspan deflection rate $\dot{\delta}$ can be expressed as the following empirical formula proposed by Adhikary et al. [31]:

$$\dot{\varepsilon} = 1.25\dot{\delta}^{0.82}. \tag{24}$$

In the overall response stage, the velocity of the system gradually reduces from V_{stab} to zero. Since it is difficult to determine the variable strain rate during the impact process, a constant value has been used for DIF in many previous studies. Similarly, the average deflection rate is used to calculate the strain rate as

$$\dot{\delta} = \frac{1}{2}V_{stab}. \tag{25}$$

Many empirical relations are available within the literature to evaluate strain rate effect on the material properties. Herein, the DIF for the compressive strength of concrete as recommended by CEB [8] is adopted, which reads as follows:

$$\text{CDIF} = \frac{f_{cd}}{f_{cs}} = \begin{cases} \left(\dfrac{\dot{\varepsilon}}{\dot{\varepsilon}_s}\right)^{1.026\alpha}, & \dot{\varepsilon} \le 30\ \text{s}^{-1}, \\ \gamma\,(\dot{\varepsilon})^{1/3}, & \dot{\varepsilon} > 30\ \text{s}^{-1}, \end{cases} \tag{26}$$

where f_{cd} is the dynamic compressive strength at the strain rate $\dot{\varepsilon}$ (MPa), f_{cs} is the static compressive strength (MPa), $\dot{\varepsilon}_s = 30 \times 10^{-6}\text{s}^{-1}$, α and γ are the two parameters given by $\alpha = (5 + 3f_{cs}/4)^{-1}$ and $\lg\gamma = 6.156\alpha - 0.49$, respectively.

Malvar and Ross [30] found that the DIF for the concrete tensile strength recommended by CEB code [8] does not fit the experimental data well. Consequently, the original formula modified by the authors with a change in slope occurring at a strain rate of $1\ \text{s}^{-1}$ instead of $30\ \text{s}^{-1}$ is adopted herein, as expressed in the following equation:

$$\text{TDIF} = \frac{f_{td}}{f_{ts}} = \begin{cases} \left(\dfrac{\dot{\varepsilon}}{\dot{\varepsilon}_s}\right)^{\delta}, & \dot{\varepsilon} \le 1\ \text{s}^{-1}, \\ \beta\left(\dfrac{\dot{\varepsilon}}{\dot{\varepsilon}_s}\right)^{1/3}, & \dot{\varepsilon} > 1\ \text{s}^{-1}, \end{cases} \tag{27}$$

where f_{td} is the dynamic tensile strength (MPa) at the strain rate $\dot{\varepsilon}$, f_{ts} is the static tensile strength (MPa), $\dot{\varepsilon}_s = 10^{-6} \cdot \text{s}^{-1}$, $\lg\beta = 6\delta - 2$, in which $\delta = 1/(1 + 8f_c/f_{c0})$ and $f_{c0} = 10$ MPa.

According to CEB code [8], taking into account the strain rate effect, the concrete ultimate strain in the compression zone can be written as

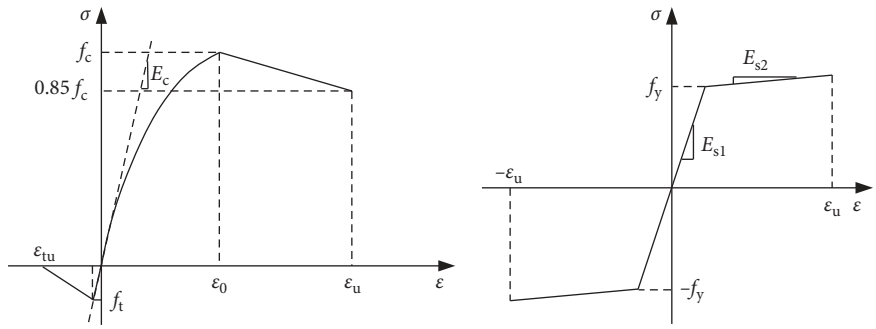

Figure 7: Stress-strain relation for materials. (a) Concrete. (b) Steel.

$$\varepsilon_{ud} = \varepsilon_{us} \cdot \left(\frac{\dot{\varepsilon}}{\dot{\varepsilon}_s}\right)^{0.02}, \tag{28}$$

where ε_{us} is the ultimate strain of concrete under static loadings and $\dot{\varepsilon}_s = 30 \times 10^{-6}\,s^{-1}$.

For reinforcing steel, the strain rate effect recommended by CEB code [8] is also utilized herein. The DIF for the yield strength is given by

$$\text{DIF} = \frac{f_{yd}}{f_{ys}} = 1 + \frac{6}{f_{ys}} \ln\left(\frac{\dot{\varepsilon}}{5 \times 10^{-5}}\right), \tag{29}$$

where f_{yd} is the dynamic yield strength (MPa) at the strain rate $\dot{\varepsilon}$ and f_{ys} is the static yield strength (MPa).

2.4.3. Moment-Curvature Diagram. In general, the nonlinear analysis of RC beams is usually conducted with the moment-curvature relationship based on the layered-section approach [1, 16, 32]. Herein, the section of the RC beam is divided into a great number of layers, as shown in Figure 8(a). Then, the curvature is calculated by assuming that the strain distribution across the section depth is linear (refer to Figure 8(b)), which means that the section remains plane under the exterior loads. According to the constitutive models of the materials and by taking into account the strain rate effect, the stress of each layer can be obtained, as presented in Figure 8(c). Finally, based on the strain compatibility and internal force equilibrium in the section, the moment-curvature relation is constructed by calculating step by step the position of the neutral axis, given a maximum concrete strain.

Figure 9 presents the moment-curvature relationship of the RC beam section, including the crack, the yield, and the ultimate state. It should be noted that its unloading behaviour is not considered in this analysis as only the maximum response of RC beams is of interest [32].

2.4.4. Force-Deflection Diagram. For the RC beam under localized impact loading, a plastic hinge is expected to be formed at the critical section in the yield and ultimate stage. Many approximate expressions for the plastic hinge length are available in the literature. In this paper, the length of the plastic hinge is estimated by the following empirical formula proposed by Mattock [33]:

$$l_p = d + 0.05 \cdot l, \tag{30}$$

where d is the effective depth of cross-section and l is the net span of the RC beam.

Based on the previously calculated moment-curvature diagram and the plastic hinge length resulted from equation (30), the force-deflection diagram of the beam under dynamic loading is finalized, as shown in Figure 10.

2.5. Maximum Deflection. Many previous studies [34] have pointed out that most of the initial kinetic energy of the impactor is absorbed by the RC beam in the overall response stage. When the midspan displacement reaches the maximum value, the common velocity of the system nearly reduces to zero. In this case, the kinetic energy in the overall response stage can be assumed to be completely converted into the internal energy of RC beams, which is equal to the area under the force-deflection curve, as illustrated in Figure 10.

At the beginning of the overall response stage (refer to point C in Figure 1), the kinetic energy $E_{k\,\text{stab}}$ of the system can be calculated by

$$E_{k\,\text{stab}} = \frac{1}{2}(M + m)V_{\text{stab}}^2. \tag{31}$$

Moreover, the energy-balanced equation with consideration given to the work of the gravity can be written as

$$E_{k\,\text{stab}} + (M + m)gs_{\max} = \int_0^{s_{\max}} F(s)ds, \tag{32}$$

where g is the acceleration of gravity, $s_{\max}$ is the maximum midspan deflection of the beam, and F is the resistance of the beam under impact loading acting at midspan.

Based on the force-deflection diagram (shown in Figure 10) and equation (32), the beam maximum midspan deflection $s_{\max}$ can be easily determined without the need to perform the impact analysis using single degree or multi-degree of the freedom system model.

3. Assessment of the Proposed Method

3.1. Experimental Database. To validate the proposed methods for predicting the peak response of RC beams discussed above, a database of 143 RC beams tested under

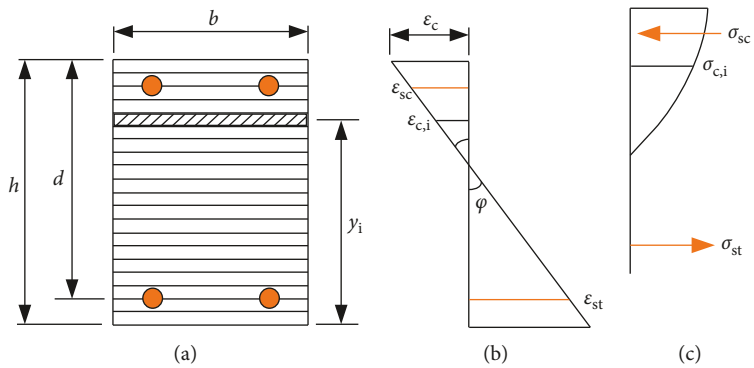

Figure 8: Section analysis. (a) Layered section. (b) Strain distribution. (c) Stress distribution.

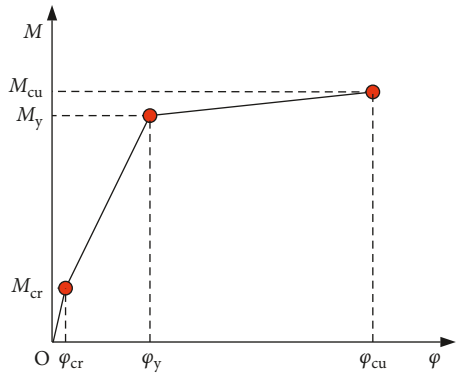

Figure 9: Moment-curvature relationship.

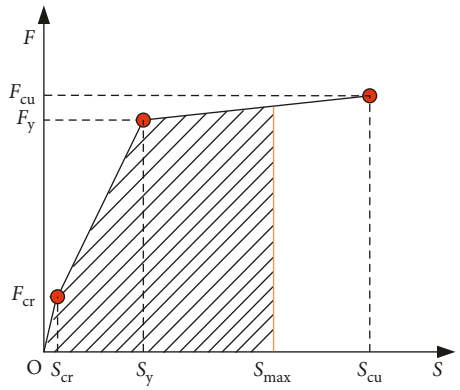

Figure 10: Force-deflection diagram of RC beams under impact loading.

drop-weight impact at midspan is compiled from other studies in the literature [1, 2, 7, 10, 35–41], as listed in Supplementary Materials (available here). All the specimens considered in this study are simply supported RC beams with rectangular cross-section, and the impactors have two types of nose shape: spherical and flat impact surface.

Figure 11 presents the parameters distribution of the collected database, such as the impact velocity, the impact mass, the geometry sizes of RC beams, the concrete compressive strength, and the amounts of longitudinal and shear reinforcement. It is apparent from Figure 11 that the impact velocity V_0 is in the range 1–16 m/s, but most of the tests are in the low-velocity impact regime. The impact mass M ranges from 100 to 1800 kg and mainly distributes between 300 and 600 kg. The RC beam width b increases from 100 to 300 mm, and the beam height h grows from 150 to 500 mm. The RC beam is simply supported over a net span 1000 to 5000 mm in length. The ratio of longitudinal tensile reinforcement is in the range of 0.25% to 3.25%, whereas the shear reinforcement ratio varies from 0 to 1.4%.

3.2. Peak Impact Force Validation. Based on the tested parameters listed in Supplementary Materials (available here), the peak impact forces are calculated using equations (17) and (18). It should be mentioned that 28 tests from the collected database lack important information about the peak impact force. Therefore, only 115 cases are adopted to validate the proposed method for calculating the peak impact force. Figure 12 compares the experimental results with the predicted results calculated by the proposed method. The peak impact forces of 92 specimens impacted by drop-weights with a spherical nose are plotted in Figure 12(a), and the peak impact forces of 23 specimens impacted by drop-weights with a flat nose are plotted in Figure 12(b). The best-fit lines for the predicted peak impact force of impactors with spherical and flat noses are $y = 1.168x$ and $y = 1.342x$, which means that there are certain deviations between the best-fit lines and the 45° benchmark. The correlation factors of the experimental results and predictions are $R^2 = 0.853$ and $R^2 = 0.929$, which indicate that the predicted impact forces generated by impactors with a flat nose are more consistent with the best-fit line than that of impactors with a spherical nose. As can be seen, most of the predictions of the peak impact force are larger than the tested results. It is primarily attributable to the fact that the elastic contact model is adopted in the proposed simplified method.

In order to intuitively compare the predictions by the proposed method with experimental results, the ratio of the predicted to the measured peak impact force (ξ) is introduced, and then a statistical analysis of ξ is conducted. For the impactors with a spherical nose, the mean value of ξ is 1.16 with a coefficient of variation of 0.217. However, overrated predictions are obtained from the cases where the impact noses are flat, and the mean value of ξ is 1.39 with a

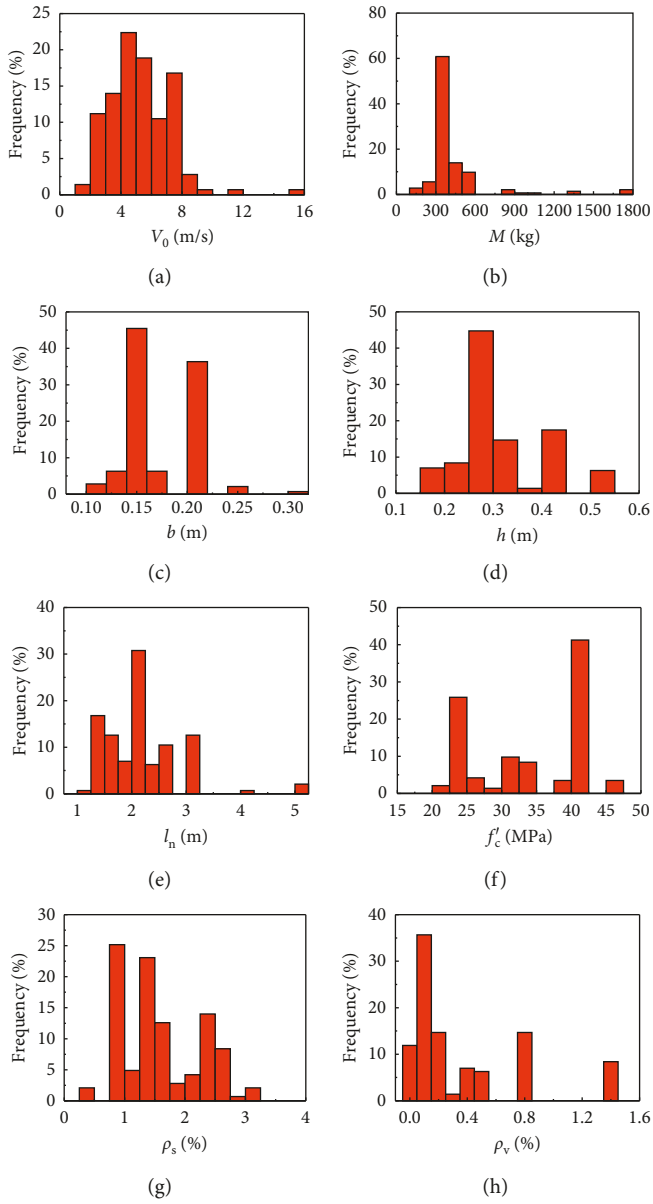

Figure 11: Distribution of the experimental parameters. (a) Impact velocity. (b) Impact mass. (c) Beams width. (d) Beams depth. (e) Net span. (f) Concrete strength. (g) Reinforcement ratio. (h) Stirrup ratio.

coefficient of variation of 0.145. Figure 13 presents the variation of ξ with the impact velocity, the impact mass, the mass ratio, and the section height. Similarly, the proposed method slightly overestimates the peak impact force, but ξ is less than 2. It can be found that the changes in the impact parameters have an insignificant effect on the overall distribution of ξ, which means the proposed method can be well applied to a wide range of these impact parameters.

Figure 14 presents the comparison of measured and predicted peak impact force using the method proposed by Pham and Hao [3]. From this figure, it can be observed that the correlation factors of the experimental results and predictions are $R^2 = 0.563$ and $R^2 = 0.343$ for spherical and flat impact noses, which indicates that the predictions of the peak impact force are not as good as that presented in Figure 12. It is mainly because the accuracy of the empirical formula strongly relies on the selected input data. Besides, the contact interface was not considered in their study, which usually has a significant effect on the impact force.

Since impact is a very complex physical problem, the contact nonlinearity, the material nonlinearity, and the dynamic effect are omitted from the proposed method in order to simplify the computational procedure. The simplified method proposed in this study is straightforward and simple and can predict the experimental results with reasonable accuracy. In addition, for RC beams susceptible to brittle shear failure near the impact position, a larger predicted peak impact force is desirable. The proposed method, therefore, appears to be a more appropriate way of calculating the peak impact force. It should be mentioned that

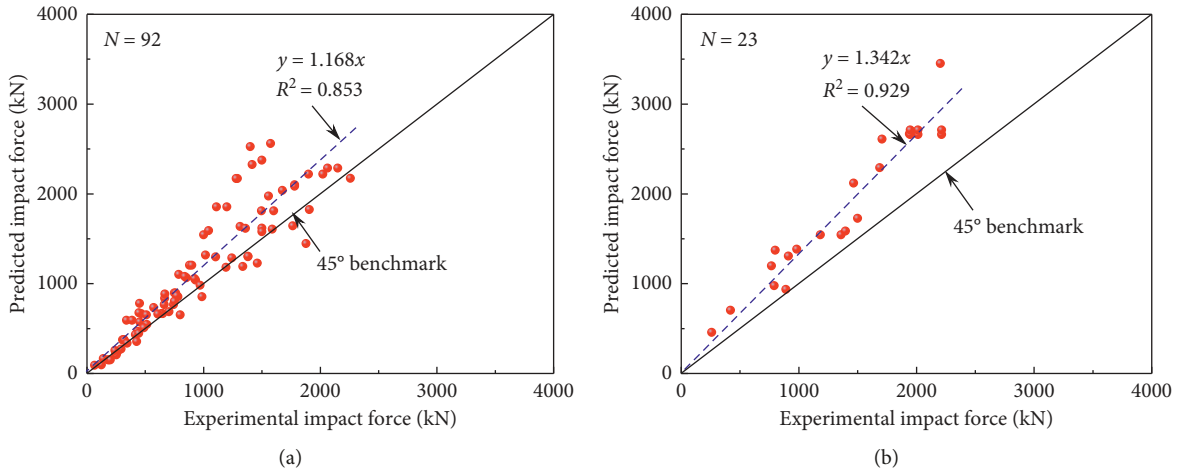

Figure 12: Comparison of experimental and predicted values of peak impact force. (a) Spherical nose. (b) Flat nose.

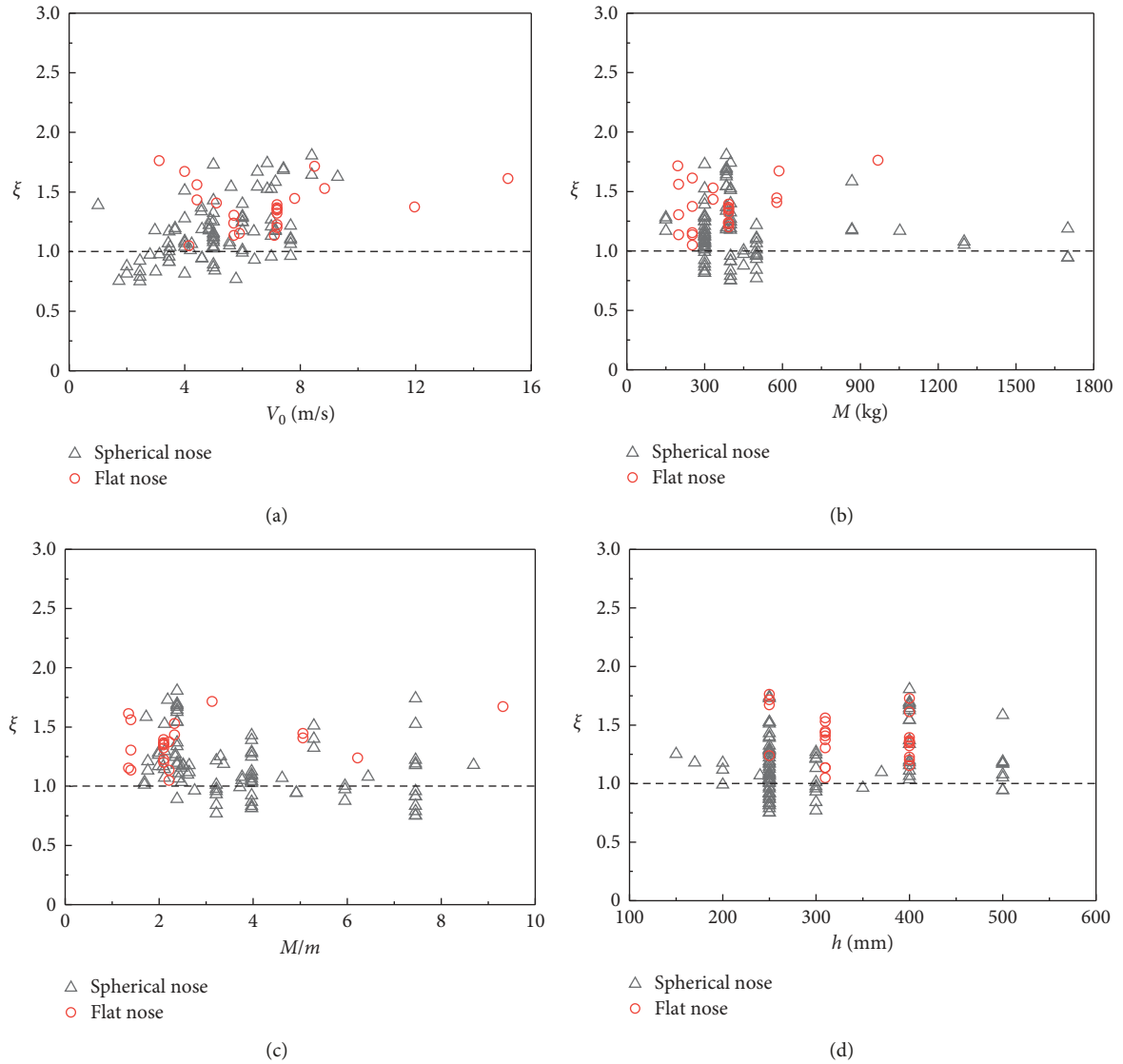

Figure 13: Influence of the main parameters on ξ. (a) Impact velocity. (b) Impact mass. (c) Mass ratio. (d) Section height.

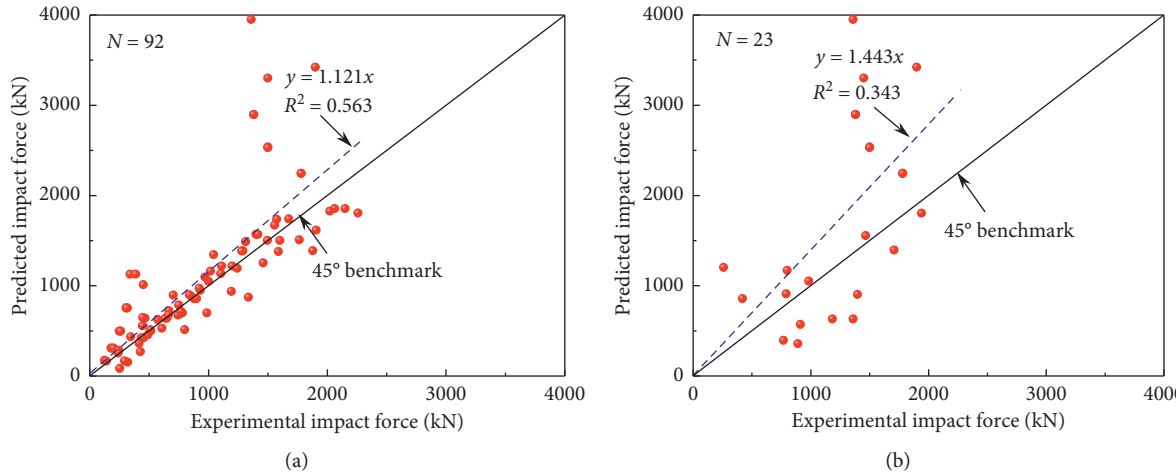

Figure 14: Comparison of experimental and predicted peak impact force using the existing method [3]. (a) Spherical nose. (b) Flat nose.

more data are required in order to further verify the application scope of the proposed method.

3.3. Maximum Midspan Deflection Validation. Since the proposed method for calculating the maximum deflection is based on the lumped midspan plastic hinge hypothesis, it is not suitable for RC beams expected to fail in shear or completely collapse. Therefore, 25 beams are eliminated from the collected database. In this case, the maximum midspan deflections of 118 RC beams under drop-weight impact are calculated by the proposed method.

Figure 15 presents the comparison of the maximum midspan deflection for the predicted and experimental results. It is shown that the proposed method can accurately predict the maximum midspan deflection of RC beams. Comparing with the predictions of the peak impact force (Figure 12), the predicted maximum deflection values have even better agreement with the experimental test results. The best-fit line, $y = 1.014x$, nearly aligns with the 45° benchmark, which indicates a strong correlation between the predicted and measured results. Similar to ξ defined previously, η is introduced here to define the ratio of the predicted to the measured maximum deflection. The average prediction-to-test ratio is 1.04 with a coefficient of variation of 0.205. The value of η mainly distributes in the range of 0.65 to 1.79. In summary, the proposed method can reproduce the impact test results with high accuracy. Evaluation of maximum deflection using the conservation of energy approach provides a simplified and physically meaningful calculation tool.

Figure 16 presents the comparison of measured and predicted maximum midspan deflection of RC beams with the formula proposed by Kishi and Mikami [10]. The correlation factor of the experimental results and predictions is $R^2 = 0.826$ that is smaller when compared to Figure 15. Since the empirical formula was established based on a part of the database complied in this study, some predicted results agree well with the experimental results, but the error of the empirical formula increases when the data are out of the specific range. It further confirms that these empirical formulas have some limitations to predict the maximum response of RC beams under impact loading.

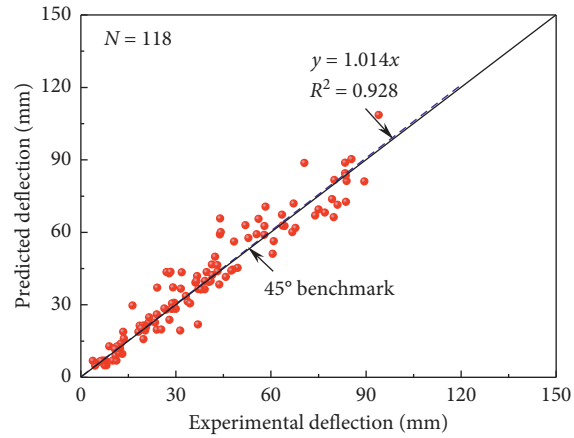

Figure 15: Comparison of experimental and predicted values of the maximum deflection.

4. Conclusions

On the basis of the preceding developments, the following conclusions can be stated:

(1) A novel and simple method for predicting the peak response of simply supported RC beams subjected to impact loading has been proposed. In contrast to the proposed method, the existing methods are inconvenient and not straightforward to be carried out, or even lack theoretical foundation.

(2) The proposed method is suitable for the impact analysis with a wide range of impact weight, impact velocity, geometric sizes, and reinforcement ratios.

(3) A comparison with 143 experimental tests has shown that the proposed method is able to estimate the midspan deflection of RC beams under impact loading with high accuracy. The peak impact force is

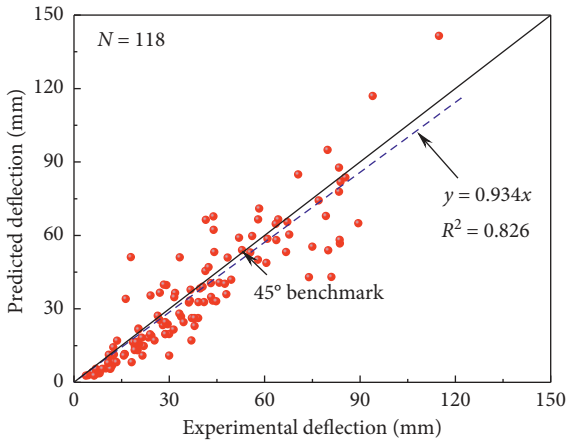

FIGURE 16: Comparison of experimental and predicted maximum deflection with the existing method [10].

shown to be slightly overestimated, which however can be used in the anti-impact design to preclude the shear failure near the impact point.

(4) Due to the straightforward nature of the proposed method and its ability to accurately predict both the displacement and impact force, it can be directly applied on the performance-based design of RC beams under impact loading.

Data Availability

The data used to support the findings of this study are included within the Supplementary Materials.

Conflicts of Interest

The authors declare that there are no conflicts of interest regarding the publication of this paper.

Acknowledgments

The authors gratefully acknowledge the financial support provided by the National Science Foundation of China under Grant no. 51438010.

Supplementary Materials

A file, named "Database.pdf," is the database collected from previous impact tests in the literature [1, 2, 7, 10, 35–41]. The compiled database consists of 143 RC beams under drop-weight impact at the midspan. Meanwhile, the beam geometric size, the material properties, the impact parameters, and the tested results are presented in detail. The database has been utilized to validate the proposed method in this paper, as shown in Figures 12–16. (*Supplementary Materials*)

References

[1] K. Fujikake, B. Li, and S. Soeun, "Impact response of reinforced concrete beam and its analytical evaluation," *Journal of Structural Engineering*, vol. 135, no. 8, pp. 938–950, 2009.

[2] S. Tachibana, H. Masuya, and S. Nakamura, "Performance based design of reinforced concrete beams under impact," *Natural Hazards and Earth System Science*, vol. 10, no. 6, pp. 1069–1078, 2010.

[3] T. M. Pham and H. Hao, "Prediction of the impact force on reinforced concrete beams from a drop weight," *Advances in Structural Engineering*, vol. 19, no. 11, pp. 1710–1722, 2016.

[4] P. Yan, J. Zhang, Q. Fang, and Y. Zhang, "Numerical simulation of the effects of falling rock's shape and impact pose on impact force and response of RC slabs," *Construction and Building Materials*, vol. 160, pp. 497–504, 2018.

[5] G. S. D. Ulzurrun and C. Zanuy, "Enhancement of impact performance of reinforced concrete beams without stirrups by adding steel fibers," *Construction and Building Materials*, vol. 145, pp. 166–182, 2017.

[6] S. Saatci and F. J. Vecchio, "Effects of shear mechanisms on impact behavior of reinforced concrete beams," *ACI structural Journal*, vol. 106, no. 1, pp. 78–86, 2009.

[7] D.-B. Zhao, W.-J. Yi, and S. K. Kunnath, "Shear mechanisms in reinforced concrete beams under impact loading," *Journal of Structural Engineering*, vol. 143, no. 9, article 04017089, 2017.

[8] Comité Euro-International du Béton, *Concrete Structures under Impact and Impulsive Loading*, CEB-Bulletin d'Information, Lausanne, Switzerland, 1988.

[9] S. D. Adhikary, B. Li, and K. Fujikake, "State-of-the-art review on low-velocity impact response of reinforced concrete beams," *Magazine of Concrete Research*, vol. 68, no. 14, pp. 701–723, 2016.

[10] N. Kishi and H. Mikami, "Empirical formulas for designing reinforced concrete beams under impact loading," *ACI Structural Journal*, vol. 109, no. 4, pp. 509–519, 2012.

[11] H. Jiang and M. G. Chorzepa, "An effective numerical simulation methodology to predict the impact response of prestressed concrete members," *Engineering Failure Analysis*, vol. 55, pp. 63–78, 2015.

[12] N. Kishi, S. G. Khasraghy, and H. Kon-No, "Numerical simulation of reinforced concrete beams under consecutive impact loading," *ACI Structural Journal*, vol. 108, no. 4, pp. 444–452, 2011.

[13] T. M. Pham, Y. Hao, and H. Hao, "Sensitivity of impact behaviour of RC beams to contact stiffness," *International Journal of Impact Engineering*, vol. 112, pp. 155–164, 2018.

[14] LS-DYNA, *Keyword User's Manual*, Livermore Software Technology Corporation, Livermore, California, USA, 2006.

[15] S. Abrate, "Modeling of impacts on composite structures," *Composite Structures*, vol. 51, no. 2, pp. 129–138, 2001.

[16] D. Bertrand, F. Kassem, F. Delhomme, and A. Limam, "Reliability analysis of an RC member impacted by a rockfall using a nonlinear SDOF model," *Engineering Structures*, vol. 89, pp. 93–102, 2015.

[17] K. L. Johnson and K. L. Johnson, *Contact Mechanics*, Cambridge University Press, Cambridge, UK, 1985.

[18] M. A. Hazizan and W. J. Cantwell, "The low velocity impact response of an aluminium honeycomb sandwich structure," *Composites Part B: Engineering*, vol. 34, no. 8, pp. 679–687, 2003.

[19] T. M. Pham and H. Hao, "Influence of global stiffness and equivalent model on prediction of impact response of RC beams," *International Journal of Impact Engineering*, vol. 113, pp. 88–97, 2017.

[20] W. J. Yi, D. B. Zhao, and S. K. Kunnath, "Simplified approach for assessing shear resistance of reinforced concrete beams under impact loads," *ACI Structural Journal*, vol. 113, no. 4, pp. 747–756, 2016.

[21] D. M. Cotsovos, "A simplified approach for assessing the load-carrying capacity of reinforced concrete beams under concentrated load applied at high rates," *International Journal of Impact Engineering*, vol. 37, no. 8, pp. 907–917, 2010.
[22] J. M. Biggs, *Introduction to Structural Dynamics*, McGraw-Hill Book Company, New York, NY, USA, 1964.
[23] T. M. Pham and H. Hao, "Plastic hinges and inertia forces in RC beams under impact loads," *International Journal of Impact Engineering*, vol. 103, pp. 1–11, 2017.
[24] P. Isaac, A. Darby, T. Ibell, and M. Evernden, "Experimental investigation into the force propagation velocity due to hard impacts on reinforced concrete members," *International Journal of Impact Engineering*, vol. 100, pp. 131–138, 2017.
[25] G. Lu and T. Yu, *Energy Absorption of Structures and Materials*, Wood-Head, Cambridge, UK, 2003.
[26] W. T. Thomson, "Transmission of elastic waves through a stratified solid medium," *Journal of Applied Physics*, vol. 21, no. 2, pp. 89–93, 1950.
[27] E. Hognestad, *A Study of Combined Bending and Axial Load in Reinforced Concrete Members*, Bulletin Series No. 399, Bulletin No.1, University of Illinois Engineering Experiment Station, Champaign, IL, USA, 1951.
[28] J. B. Mander, M. J. N. Priestley, and R. Park, "Theoretical stress-strain model for confined concrete," *Journal of structural engineering*, vol. 114, no. 8, pp. 1804–1826, 1988.
[29] FIB 2010, *Fib Model Code for Concrete Structure 2010*, Wiley-VCH Verlag GmbH & Co. KGaA, Weinheim, Germany, 2013.
[30] L. J. Malvar and C. A. Ross, "Review of strain rate effects for concrete in tension," *ACI Materials Journal*, vol. 95, no. 6, pp. 735–739, 1998.
[31] S. D. Adhikary, B. Li, and K. Fujikake, "Dynamic behavior of reinforced concrete beams under varying rates of concentrated loading," *International Journal of Impact Engineering*, vol. 47, pp. 24–38, 2012.
[32] G. Carta and F. Stochino, "Theoretical models to predict the flexural failure of reinforced concrete beams under blast loads," *Engineering structures*, vol. 49, pp. 306–315, 2013.
[33] A. H. Mattock, "Discussion of rotational capacity of reinforced concrete beams," *Journal of the Structural Division*, vol. 93, no. ST2, pp. 519–522, 1967.
[34] B. P. Hughes and H. Al-Dafiry, "Impact energy absorption at contact zone and supports of reinforced plain and fibrous concrete beams," *Construction and Building Materials*, vol. 9, no. 4, pp. 239–244, 1995.
[35] A. Q. Bhatti, N. Kishi, H. Mikami, and T. Ando, "Elasto-plastic impact response analysis of shear-failure-type RC beams with shear rebars," *Materials and Design*, vol. 30, no. 3, pp. 502–510, 2009.
[36] S. D. Adhikary, B. Li, and K. Fujikake, "Low velocity impact response of reinforced concrete beams: experimental and numerical investigation," *International Journal of Protective Structures*, vol. 6, no. 1, pp. 81–111, 2015.
[37] L. Jin, R. Zhang, G. Dou, J. Xu, and X. Du, "Experimental and numerical study of reinforced concrete beams with steel fibers subjected to impact loading," *International Journal of Damage Mechanics*, vol. 27, no. 7, pp. 1058–1083, 2017.
[38] X. Zeng and B. Xu, "Experimental study on the impact-resistant behavior of RC beams without shear-resistant rebar," *China Civil Engineering Journal*, vol. 45, no. 9, pp. 63–73, 2012, in Chinese.
[39] B. Xu and X. Zeng, "Experimental study on the behaviours of reinforced concrete beams under impact loading," *China Civil Engineering Journal*, vol. 47, no. 2, pp. 41–51, 2014, in Chinese.
[40] D.-B. Zhao and W.-J. Yi, "Anti-impact behavior and design method for RC beams," *Journal of Vibration and Shock*, vol. 34, no. 11, pp. 139–145, 2015, in Chinese.
[41] G.-Q. Dou, X.-L. Du, and L. Li, "Experimental study on the behavior of high strength reinforced concrete beams under impact load," *Journal of Tianjin University(Science and technology)*, vol. 47, no. 12, pp. 1072–1080, 2014, in Chinese.